Research Square

Preprints are preliminary reports that have not undergone peer review.
They should not be considered conclusive, used to inform clinical practice,
or referenced by the media as validated information.

A Configurable VR Spacecraft Simulator enhanced with HMI data in Microgravity

Ajit Krishnan
Indian Institute of Science
Himanshu Vishwakarma
Indian Institute of Science
Siddhant Thalal
Indian Institute of Science
Suprakas Saren
Indian Institute of Science
Maharudra Kharsade
Indian Institute of Science
KamalPreet Singh Saluja
Indian Institute of Science
Mukund Mitra
Indian Institute of Science
Pradipta Biswas
pradipta@iisc.ac.in

Indian Institute of Science

Article

Keywords:

Posted Date: June 4th, 2026

DOI: https://doi.org/10.21203/rs.3.rs-9697554/v1

License: This work is licensed under a Creative Commons Attribution 4.0 International License.
Read Full License

Additional Declarations: No competing interests reported.

A Configurable VR Spacecraft Simulator enhanced with HMI data in Microgravity

Ajit Krishnan, Himanshu Vishwakarma, Siddhant Thalal, Suprakash Saren, Maharudra Kharsade, KamalPreet Singh Saluja, Mukund Mitra, Pradipta Biswas[1]

Indian Institute of Science, Bangalore 560012, India

[1]Corresponding Author, Email: pradipta@iisc.ac.in

Abstract: Simulators play a crucial role in the aerospace industry, ranging from simple desktop models to advanced Level D simulators used for pilot training. While most non-gaming simulators focus on crew training and client illustration, there is a notable deficiency in simulators that assist with cockpit design. Current methods primarily utilize standard CAD/CAE software alongside Digital Human Models, which often lack adequate functionality for comprehensive human factor evaluation for design optimization. This paper introduces a configurable Virtual Reality Spacecraft Simulator that is calibrated with data from microgravity studies. Unlike manned aircraft, operations involving spacecraft and rovers are predominantly automated or controlled from the ground. The NASA Human Rating standard underscores the importance of manual flight control for crew safety during unexpected failures, with historical missions demonstrating how manual control can ensure safe returns. Therefore, spacecraft simulation must encompass experiences within the craft, similar to how aircraft crews train in high-gravity conditions. Microgravity simulations on Earth, typically lasting less than 30 seconds, are insufficient for thorough human-machine interaction studies. The proposed VR simulator is enhanced by data from the International Space Station, enabling immersive task execution in scenarios such as deorbiting manoeuvres, emergency responses, and robotic arm operations, while also predicting task completion times in microgravity conditions.

1. Introduction

Simulators are essential part of AeroSpace industry ranging from basic desktop or gaming simulator to level D simulators for pilot training. Majority of non-gaming simulators are developed for pilot/crew training or illustration to customers. However, there is a serious gap in Aerospace simulators to aid in cockpit design process. Existing practice uses standard CAD/CAE (Computer Aided Design/Engineering) packages along with Digital Human Models. However, often a CAD/ CAE models do not offer enough functionalities to be evaluated or experienced by humans. This paper presents a configurable Virtual Reality Spacecraft Simulator calibrated with data from microgravity study.

Unlike manned aircraft, spacecraft or extraterrestrial rover operations are mostly automated or ground-controlled. However, the NASA Human Rating standards makes it mandatory to have manual control for human rated space flights and the Robotic Work Station (RWS) on-board the International Space Station is used for time-critical operations such as visiting vehicle captures using Canadarm2. [NASA 2017]. Historical missions, including Mercury 9, Gemini 4, Gemini 8, and Apollo 13, illustrated the effectiveness of manual controls in ensuring safe returns. This approach not only enables crews to override malfunctioning automation but also contributes to weight savings by eliminating redundant automatic systems.

For spacecraft simulation, we need to consider operations inside a spacecraft or space station in microgravity environment. Aircraft crews are regularly trained in sustained high-Gravity situations with centrifuges. Spacecraft simulation should similarly be calibrated with microgravity simulation data. On earth, the best microgravity simulation for humans is obtained through parabolic flight, which presently offer a maximum 30 secs of sustained microgravity. This small duration is not enough to undertake user study on human machine interaction. The NASA VR Lab uses robotic arms to simulate object handling experience in microgravity. We calibrated the proposed VR simulator with data collected at the International Space Station. The overall system allows to undertake different tasks in an immersive environment like deorbiting manoeuvre, emergency response, robotic arm operation under different settings with prediction of task completion times under microgravity.

2. Literature Survey

The evolution of manual flight control in manned spacecraft demonstrates a consistent emphasis on ensuring human override capability alongside increasing automation. Early spacecraft such as Vostok and Mercury relied primarily on automatic control, with limited manual intervention mainly for attitude adjustment and de-orbit operations using simple hand-operated controllers and periscope-based Earth references [Hendrickx 2018, Maksimov 2011]. Subsequent systems like Gemini marked a significant transition, introducing mission-critical manual tasks such as rendezvous, docking, and re-entry control, supported by improved human-machine interfaces and window-based visual cues [Ney 1966]. Later spacecraft including Apollo and Soyuz retained both automated and manual modes, expanding manual capabilities to include translational control, power-generation orientation, and docking operations [Volf 2021]. Visual references evolved into two dominant paradigms: full Earth-circumference views (periscope-based) and forward-facing window views resembling aircraft cockpits. Modern spacecraft such as Crew Dragon introduce a paradigm shift by replacing traditional hand controllers with touchscreen interfaces [Jones 2024], although core manual control tasks remain consistent. Spacecraft simulators evolved from flight simulators following the required functionalities of a spacecraft.

2.1. Spacecraft Simulator

Flight simulators have long been integral to pilot training in both commercial and military sectors, providing crucial experience with complex aircraft systems. Yet, traditional simulators often lack adaptability and are specific to certain aircraft. Virtual Reality (VR) emerges as a potential supplementary tool, enhancing training immersion without fully replacing existing simulators. Spacecraft simulators are broadly classified as [Wilde 2019; Granados-Cruz 2023]

- **Kinematic Simulators**: Focus on translational or rotational motion using actuators that may not be flight-representative. They are often used for testing orbital lighting and sensor accuracy.
- **Dynamic Simulators**: Reproduce the actual physical forces (torques and forces) experienced in space. These often use self-contained vehicles to avoid dynamic interference from the environment.
- **Hybrid Simulators**: Combine robotic manipulators (kinematic) with dynamic decoupling elements, such as air-bearing floors, to simulate interactions like capturing or docking.

- **Kino-dynamic Simulators**: Attempt to reproduce dominating dynamic properties while overcoming the physical limitations of degrees of freedom (DOF) and mass typically found in air-bearing systems.

It may be noted that most existing reviews [Wilde 2019; Granados-Cruz 2023] do not include separate category for human machine interface simulators except simulators used for crew training. A report [Metodi 2010] on Space Vehicle Testbeds and Simulators prepared for US Air Force Space Command introduces a standardized taxonomy that classifies Testbeds & Simulators based on end users, end uses, functional capabilities, and physical characteristics. Figure 3-1 and Table 3-1 in the report identified different stakeholders for spacecraft simulators, which do not explicitly include designers for cockpit or human machine interfaces. In the context of spacestation operations, particularly the International Space Station (ISS) and the forthcoming Lunar Gateway, simulation plays a crucial role, especially in proximity manoeuvres and robotic interactions. The SPHERES platform [SPHERES 2016] on the ISS serves as a six-degree-of-freedom internal simulator, enabling the study of autonomous navigation and cooperative robotics in a microgravity environment. Additionally, the Artemis program employs modern virtual reality simulators to assess complex docking systems, facilitating the transition between rotation and latching during docking and undocking processes [Artemis 2026]. India's Space Docking Experiment (SpaDeX) conducted by ISRO (Indian Space and Research Organization) recently validated autonomous docking and refuelling through orbital testbeds, marking an essential step toward the development of the Bharatiya Antariksh Station [BAS 2026]. In summary, most Virtual Reality (VR) spacecraft simulators are used for following purposes.

- **Astronaut Training:** Systems like NASA's VR lab [2026] simulate hazardous tasks, such as spacewalks (EVA), allowing trainees to experience microgravity environments. However primary purpose of the simulator is training and giving experience of object handling in microgravity.
- **Mission Planning:** Simulations provide realistic views of planetary surfaces and spacecraft trajectories, essential for planning complex manoeuvres.
- **Collaborative Training:** Recent literature highlights a trend toward collaborative VR flight simulators, addressing the gap in multi-crew cooperation (MCC) training which was previously limited to single-pilot setups. [Cross 2025]

Why we need a separate HMI simulator beyond crew training? The literature survey shows significant variations in HMI controls in spacecrafts from different nations like the periscopic view orientation by Russian spacecrafts versus windscreen style front view preferred by American spacecrafts. Space travel is opening to a diverse population beyond highly trained test pilots. On 27th April 2026, ISRO announced selection of civilians for next phase of astronaut selection while NASA and Blue Origin already ferrying civilian mission specialists and tourists to space. Private players like SpaceX are experimenting newer HMI like touchscreen in Dragon Crew. In near future, manned Lunar and Planetary missions will explore versatile operations like launch, docking and surface operations. There is a clear gap on use of a spacecraft simulator for design optimization of human machine interfaces. There is also not much reported work on calibrating or coupling VR spacecraft simulator on earth with actual data on human machine interaction in a spacecraft or spacestation. The following section discusses human machine interaction studies undertaken in microgravity environments

2.2. HMI in Microgravity Environment

We act in various ways of moving our various body parts like walking, running, nodding head, hand gesturing and so on. In the field of HMI, we concentrate on a particular type of movement known as rapid aiming movements, which include operating touchscreen, touchpad, physical bezel keys or keyboard buttons. Analysis of rapid aiming movement has a rich history starting from last decade of 18th century, when Woodworth [Eliott 2001] was inspired by the speed and accuracy of hammering activity of construction workers. Woodworth's doctoral dissertation concluded that with visual feedback people make more error with higher speed of execution while without visual feedback, error does not depend on accuracy. The finding leads to two phases of rapid aiming movement – the ballistic phase that does not depend on visual feedback and the homing phase that depends on visual feedback. Later in 1954, Paul M Fitts' published a seminal paper where he predicted the task completion time as a function distance to target and width of target [Fitts 1954]. In 1979, Stuart Card used Fitts' Law to predict mouse as the most efficient pointing device compared to joystick and head movement tracker based on which Xerox Parc and later other companies started to market computer mouse [MacKenzie 2018]. Later the Fitts' Law task became part of ISO 9241 standard [ISO 9241-303, 2011] and presently used to compare or evaluate any pointing device. Besides numerous terrestrial applications, Fitts' Law study was also conducted at the International Space Station [Holden 2023]. Holden's study was an elaborate well-designed study involving seven astronauts and four tasks spanning more than three months. For pointing tasks, the study used two different target sizes. Holden found that performance was degraded during gravity transitions (first week on orbit, return to Earth) but did not find any significant difference in pointing performance between ISS and ground crews after first week of stay in the ISS. Ciofani [2012] reported results from a Fitts' Law task undertaken during parabolic flight at both hypergravity (1.8G) and microgravity from four participants. Authors reported more variance in movement times in microgravity and hypergravity conditions compared to control condition of 1G. Authors fit a third order polynomial between movement time (MT) and Index of Difficulty (ID) for hypergravity and microgravity conditions. Bieg [2024] reported results from a touchscreen tapping task at a head-down tilt (HDT) bed rest as part of the Artificial Gravity Bed Rest, European Space Agency (AGBRESA) at the German Aerospace Center (DLR) in Cologne. Researchers reported validity of Fitts' Law in HDT condition in terms of regression parameters between movement time and Index of Difficulty (ID) with slopes ranging from 143 to 163 and R^2 ranging from 0.94 to 0.96 using data collected from 24 healthy participants aged 24 to 55 years. In conclusion, we did not find any reported work on Fitts' Law study in sustained microgravity environment involving different target sizes and distances.

3. Virtual Reality Simulator Design

A virtual spacecraft cabin model was developed in Unity 3D to represent a reconfigurable interior environment for simulation and interaction (Figure 1). The model defined a structured cabin layout with measurable dimensions and included functional elements such as console, seating, and onboard systems. Appendix 1 listed a set of existing VR spacecraft cockpit which are exact replica of previous missions. The present simulator emphasized on reconfiguration and is not a direct replica of any existing or future spacecraft. Unity 3D gaming engine was used to create and manage the scene, allowing object placement, coordinate-based measurement, and interaction through a VR interface. The system was intended to support visualization, operator interaction, and modification of cabin configuration based on mission

requirements. The cabin geometry was defined within the Unity environment using a fixed coordinate frame. The dimensions are 3.63 m along the X-axis, 1.87 m along the Y-axis, and 3.63 m along the Z-axis. Based on these values, the internal volume of the cabin is approximately 24.67cubic m. This volume defined the available space for placing equipment and seating elements while maintaining a bounded environment.

3.1. Interior of the Crew Module

The visual interface was implemented using two consoles placed in front of the seating area. The consoles were oriented at an angle of 45° with respect to the seats. It included two interactive canvases with peripheral buttons like bezel keys of a Multi-Function Display (MFD) that allowed user input during operation. The configuration supported visualization of images and live data streams, and interaction is handled through the VR controller. The placement and orientation of the console were defined within the Unity scene to maintain consistent alignment with the user's field of view during interaction. Two seats were positioned in front of the console. The seats were aligned to provide direct visibility of both canvas display. The seating system was configurable through a VR controller, allowing the user to switch seat positions during runtime. This enabled changes in user viewpoint and interaction without modifying the scene structure. The seat positions were defined relative to the cabin coordinate system and could be updated dynamically based on user input.

The cabin included components representing onboard systems and safety elements. These included two attenuators for vibration or noise control, two Air Revitalization System (ARS) canisters for maintaining breathable air conditions, and two emergency safety kits. In addition, three fans were mounted above the seating area. The fans were attached to the rigid body structure of the cabin. All components were placed as individual objects within the Unity environment and were referenced through the scene hierarchy. The interior layout allowed reconfiguration by utilizing available space within the cabin. Objects could be added, removed, or repositioned based on defined requirements. This supported variation in cabin setup without changing the base geometry. The model was operated within a coordinate-based framework, enabling consistent placement and adjustment of elements. The implementation in the Unity 3D integrated geometry, object placement, and VR-based interaction within a single environment. The system provided a platform for evaluating cabin layout, interaction mechanisms, and component arrangement under controlled conditions.

An alert alarm system was integrated into the spacecraft simulation to notify users during abnormal or critical operating conditions. A repetitive sound with a frequency of 2 Hz was used to provide a clear and recognisable emergency warning signal following Mil1472G standard. The alert sound is configurable between spoken and non-spoken (like beep-beep) sounds. Unity's spatial audio sound library was utilised to provide realistic auditory feedback within the virtual environment.

3.2. Exterior of the Crew Module

A spherical virtual asset resembling the Earth with a mass of 6115.52 kg, radius of 6378 Km rotating at 15.04° per hour simulating Earth's axial rotation was modelled. A light source simulating the Sun was placed at the farthest distance from Earth that the gaming engine permitted. The spacecraft was positioned at 400 km altitude aligned with Local Vertical Local Horizontal (LVLH) given an initial horizontal velocity of 7.6 km/s prograde.



Figure 1. The Virtual Reality Simulator Set Up

3.3. Tasks

The VR simulator was equipped with a human factor evaluation toolset. It was deployed on an HTC Vive Pro Eye headset with in-built eye gaze tracker. A 32 electrode EEG tracker was integrated through bespoke software to synchronously record ocular and EEG parameters while participants undertook tasks. Continuous log of current attitude error with respect to the reference, fuel and eye tracking data was recorded from the VR simulation. Appendix 2 at the end of the paper elaborated the human factor analysis tools. Based on literature survey on human intervention required in spacecraft operation, the following tasks were implemented.

1. **Deorbiting Maneuver:** De-orbit requires more precision than any other typical on-orbit task other than docking. In our implementation, the spacecraft was oriented with an initial configuration of pitch 0^o, bank 102^o and heading 104^o with respect to de-orbit attitude at the start of simulation. In this attitude a portion of Earth was visible in either of the cameras. The pilot was required to achieve de-orbit attitude using the control stick within an accuracy of 1° pitch, 1° roll and 6° yaw. Pilot flying the simulator could manipulate orientation of the spacecraft by demanding rotation about body axes. The console displays included a virtual horizon line, a pitch ladder, a heading scale, numeric indicators of body rates and body angles with respect to a reference coordinate system, current fuel available and manual method of altitude determination based on the size of the Earth disk on crew display. Two reference coordinate systems were defined and used – Local vertical local horizontal (LVLH), Sun. When the body axes were aligned with 'LVLH' the spacecraft was in prograde orbit raising burn attitude.
2. **Robotic Operation:** This task allows to remotely control robotic arms from VR environment. Teleoperation in VR is enabled through real-time mapping of user inputs from touchpad of handheld controllers or onscreen buttons to robot motion commands. The control law utilizes a circular touchpad or onscreen segmented into multiple sectors, each corresponding to a specific

directional motion command for the robot. User selection of a sector directs the robot's movement, with the contact duration determining the motion magnitude for smooth control. Additionally, a retraction mechanism is incorporated to allow the robot to return to its initial position by reversing along the chosen path, thus ensuring a straightforward method for both actuation and recovery of the robot's configuration. User input is transmitted via WebSockets to a remotely located microcontroller, which actuates the robot's motors. The resulting motion is reflected in the VR workspace, while a motion capture system tracks the robot and provides continuous feedback for visualization. This closed-loop interaction enables intuitive and responsive control of the robot within the immersive VR environment.

3. **Console Monitoring:** The task has live graphs in a virtual setting including configurable font sizes and line widths. The VR environment had two graphs setting each on the left and right side. The graph was similar to a line graph which changed over the time, users would observe some anomaly in the line width of the graph. Multiple anomalies at pre-designated or random intervals could be configured in each graph. The distance between virtual console and eye was maintained in range 60-65 cm in VR.
4. **Emergency Response:** Emergency response is one of important actions requiring human intervention. During spacecraft operations across different phases—launch, orbit, and landing—certain buttons are instrumental for monitoring and managing various systems. The proposed simulator has two consoles, the peripheral bezel keys and buttons between consoles are configured to respond to emergency situations during ascent, descent or orbital phases. The sequence of actions includes checking environmental parameters, setting up communication with telemetry data, manually controlling the spacecraft or abort launch sequence and so on. The sequence can be configured based on phases and can be used to predict time as well as train crew on practicing emergency sequence.

A simulator developed for only training purposes has most of its features standardized and frozen. The proposed simulator is developed for design optimization to be used primarily by designers. The following sections discuss a set of adjustment or personalization techniques implemented in the simulator that can be used by any of the tasks discussed above.

3.4. Hardware Adjustment

The VR simulator is integrated to three types of manoeuvring control based on literature survey of past and existing HMIs of spacecrafts (Table 1). The simulator is integrated to a 3-DoF flight stick, a bespoke physical switch and virtual haptic switch resembling touchscreen controls. A Thrustmaster 16000T three-axis control stick is configured with a linear control law, where the neutral position corresponds to 0°/sec and deflection corresponds to a maximum of 3°/sec at full deflection. It features a spring-loaded mechanism that ensures a null rate demand initially. Additionally, a bespoke physical switch system comprised of six keys, each affecting the rate by ±1°/sec, with a maximum clamped rate of +3°/sec is integrated for pitch, roll and yaw control. The physical switch used an ESP32 microcontroller, utilizing pull-up logic, detects button presses by transitioning pins from HIGH to LOW when switched, facilitating communication with a web server that broadcasts access points upon power-up. For virtual touch, the Manus prime 3 haptic XR glove integrated with an HTC Vive tracker enabled manual attitude control of the spacecraft by facilitating virtual touch interactions. The hand model, tracked for position and orientation, provides haptic feedback through a collider generator and is designed to respond to button activations

similarly to the physical switches, translating touch inputs into angular rate measurements between -3 and +3, indicating the corresponding rate of change in angular position.

Table 1. Different Types of External Views and Manoeuvring Controls used in Spacecrafts

SPACECRAFT	EXTERNAL VIEW			CONTROL METHOD		
	Window	Camera	Periscope	3 Axis Stick	Physical Button	Touchscreen keys
Vostok	✔		✔	✔		
Voskhod	✔		✔	✔		
Mercury	✔			✔		
Gemini	✔			✔		
Apollo	✔			✔		
Soyuz	✔	✔	✔	✔	✔	
Shenzhou	✔	✔	✔	✔	✔	
Crew Dragon	✔	✔				✔
Orion	✔	✔		✔		
CST-100	✔	✔		✔		

A previous study [Krishnan 2025] involving the VR simulator compared the three control interfaces with respect to deorbiting manoeuvre of a spacecraft. Crew performance was evaluated using metrics such as task completion time, fuel consumption, cognitive workload, and user preference. Results showed that the flight stick enables faster manoeuvring, while physical buttons are more fuel-efficient. However, virtual buttons perform poorly due to limitations in depth perception and interaction fidelity.

3.5. View Adjustment

The proposed VR simulator offered adjusting views both inside and outside the simulator. For inside view, operators can change internal lighting and colour of inner wall. The VR simulator incorporated two distinct lighting control mechanisms to enhance user interaction and environmental customization (Figure 2).

The first mechanism was based on material switching, where predefined wall materials were applied to simulate different lighting conditions without modifying the actual Unity light components. In this approach, Function 1 (White) produced a neutral, bright appearance, while Function 2 (Brown) created a warmer ambient effect.

The second mechanism utilized an interactive slider to control lighting intensity dynamically based on its position. A virtual slider was used to control the lighting intensity parameter of the environment in virtual scene. At the minimum slider value, the environment appeared dim, and the brightness was increased progressively as the slider moved toward its maximum range. Its positional value was mapped to the brightness level of the environment, enabling continuous adjustment of illumination. At the minimum slider position, the system applied low-intensity lighting to create a dim ambience. As the slider value

increased, the light intensity was proportionally increased in real time. At the maximum position, full brightness was achieved, resulting in maximum scene illumination. In Unity, HDRP (High-Definition Render Pipeline) with Physical Light Units enabled, the light intensity can use real units such as Lux (Directional Light), cd/m² (emissive surfaces).

For a standard setup, the mapping can be expressed as:

$$I = I_{min} + \left(\frac{S - S_{min}}{S_{max} - S_{min}}\right)(I_{max} - I_{min})$$

Where:

- S= slider value
- I= resulting light intensity
- I_{min}, I_{max}= defined intensity range

For example, a slider from 0–1 could be mapped to 0–500 lux for room lighting simulation. This dual-mode approach enables both preset ambience selection and continuous real-time brightness adjustment within the virtual environment.

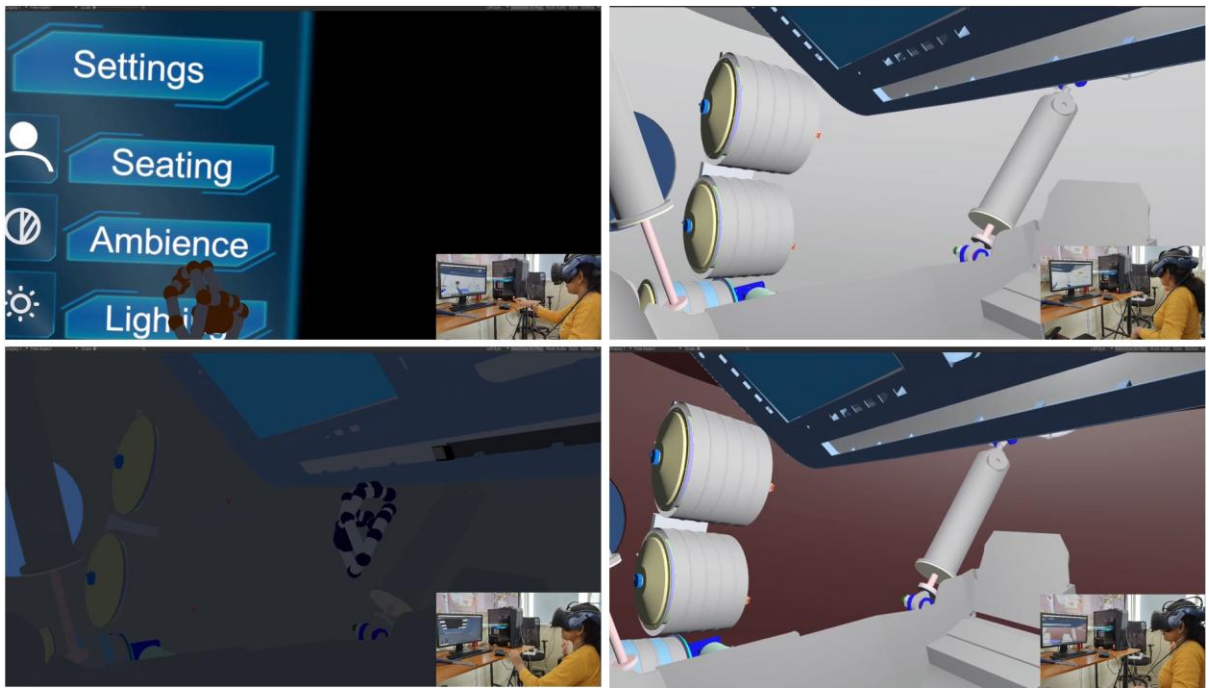


Figure 2. Different View of Inner Wall and Illumination Level inside the VR Simulator

The VR simulator also implemented two different ways to look outside the VR crew module following past spacecraft designs (Figure 3, Table 1).

- **Bottom View:** This view orientation was inspired by Russian spacecraft design like Vostok or Soyuz. A camera was positioned on the body of the VR simulator with 145 X 145 deg FOV (Field of View). This camera could capture the entire Earth disc in de-orbit attitude. Another camera bore-sighted

along Yg with 40° X 40° FOV was co-positioned. This camera permitted appreciation of direction of motion by viewing the terrain below.

- **Front View:** This view orientation was inspired by American spacecrafts like Gemini, Apollo or Crew Dragon. A camera was positioned on the body of the VR simulator with 70° X 70° FOV (Field of View) bore-sighted along Z_g. This camera would permit viewing an arc of the horizon in de-orbit attitude.

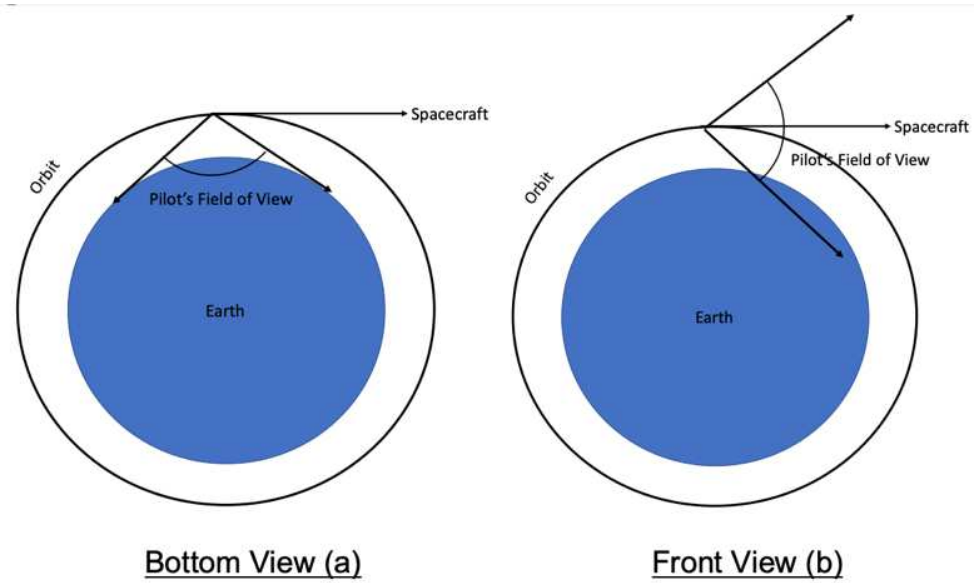


Figure 3 Two types of external view supported in the VR Simulator

Operators could choose whether to use bottom or front camera. Suitable HMI overlay was provided for accurate attitude establishment. The HMI included a virtual horizon line, a pitch ladder, a heading scale, numeric indicators of body rates and body angles with respect to a reference coordinate system, current fuel available and a manual method of altitude determination (only for bottom view) based on the size of the Earth disk on crew display. Two reference coordinate systems were defined and used – Local vertical local horizontal (LVLH), Sun. When the body axes were aligned with LVLH the spacecraft was in prograde orbit raising burn attitude. Body axes aligned with the Sun resulted in power generation attitude. Crew could select the desired reference system using keypad keypress. Suitable UI marks were made on the display to assist in correctly positioning the Earth where required. Drift markers were provided on the bottom view zoom display (selectable by player).

3.6. Console Personalization

Personalization of interfaces in VR applications allows users, specifically virtual astronauts, to tailor displays to their individual needs by adjusting factors such as font size, contrast, and colour schemes. This customization facilitates easier access to critical information for all crew members, thereby minimizing errors and enhancing navigational confidence.

In the proposed VR simulator, users could modify settings of the console displays through XML files, allowing for quick adjustments without the need to reopen or rebuild the application (Figure 4). Users can modify visual elements such as font size and colour, console background to enhance readability and usability. The VR simulator also supported dark adaptation as specified in Mil 14472G [2012] and NASA

HMI standards [NASA 2025]. Users could also create personalized XML profiles those supported a plug-and-play functionality in Unity-developed interfaces, with buttons linked to specific script functions for the desired changes in the user interface.

The console personalization process consisted of four stages: 1) Creating an XML file to define various attributes such as font sizes (12, 14, 16), text colours (black, white), and background colours (black, cyan); 2) Developing classes for each feature to assign variables to XML tags; 3) Creating a colour object with assigned R, G, B and Alpha values; and 4) Utilizing the *GetComponent* function to access text elements and assign XML values from the class. C# classes were defined to represent these attributes, including FontXml and multiple colour classes for ARGB data. XML files were integrated into the Unity project, with scripts attached to scene objects to streamline text and background property assignments. The method automated the detection of text fields, allowing new entries to be tagged for efficient processing without repetitive manual input.

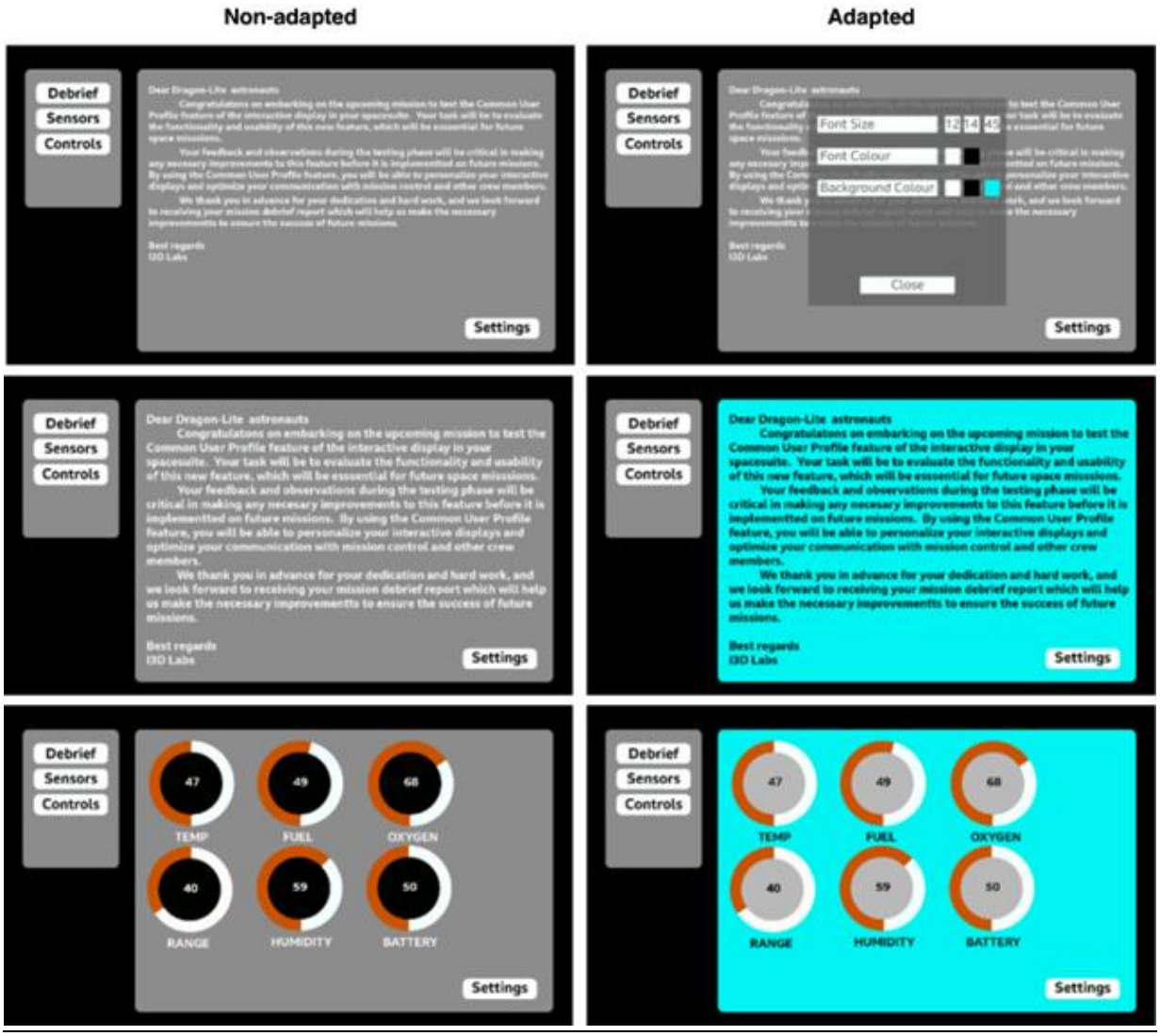


Figure 4. Examples of Personalization in terms of font size and colour contrast for a console page

3.7. Human Robot Interface (HRI) Adjustment

Automated robots are already common in terrestrial manufacturing processes helping in assembly/disassembly of components, transportation of inventory across factory floors, site maintenance, asset tracking and so on. Space robotics is predominantly automated but there are multiple situations that require the precision of human dexterity or situational awareness for decision making. Current space manipulators (CanadaArm2, ERA, JAXTA Arm) at the International Space Station rely on multiple camera views from sensors mounted on the arm. There is also a provision of visual feedback through a window in ISS when the arm is operated from there. However multiple monitors take significant physical space and specialized training for operators. The VR simulator (Figure 5) features following three interfaces for real-time control and visualization of the robotic system.

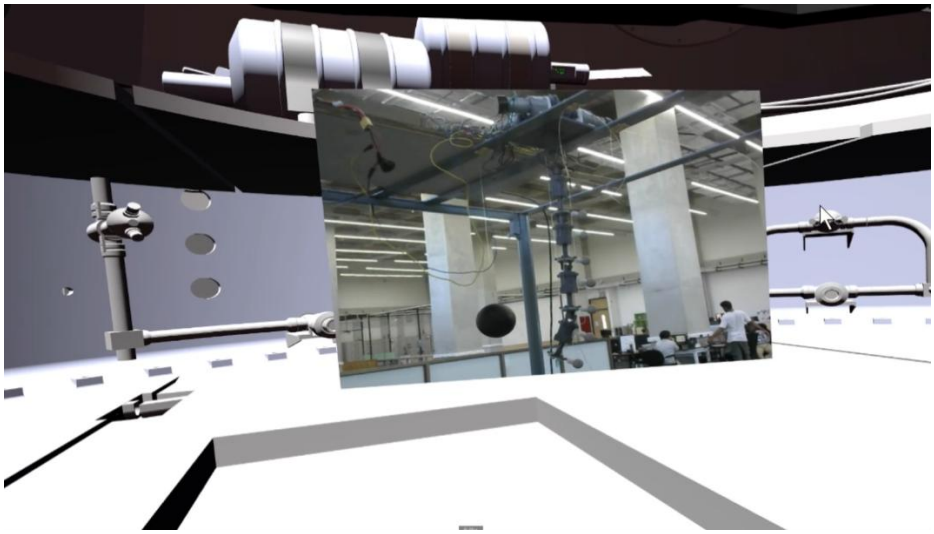
VR-based interface: The VR-based interface used a virtual camera with a field of view of 60° vertical and 84.07° horizontal. The operator was positioned 1.12 m from the virtual workspace at the initial position and could move within the interface during operation. A robotic manipulator was represented using a Unified Robot Description Format (URDF)-based structure consisting of a base link and four cylindrical links arranged in a serial configuration. The model was scaled by a factor of 0.2 within the virtual environment. Accordingly, the base link had dimensions of 0.08 × 0.08 × 0.01 m, and each cylindrical link has a length of 0.1 m and a radius of 0.01 m. The cylinders were color-coded for visual distinction. Between each pair of links, two revolute joints about the x and y axes and one prismatic joint along the z-axis were defined using intermediate links. The revolute joints had limits from −85° to 85°, and the prismatic joints provided linear actuation along the z-axis. Spherical balls were displayed within the virtual workspace.

Camera-based interface: The camera-based interface used live video feedback from an external camera positioned approximately 90 cm from the robot to ensure that the entire workspace was clearly visible within its field of view. The video stream was displayed on a Unity UI canvas with dimensions of 0.5 × 0.4 (world units). The operator was positioned 1.01 m from the canvas. A physical ball was placed within the workspace as a representative target and was visible through the camera feed.

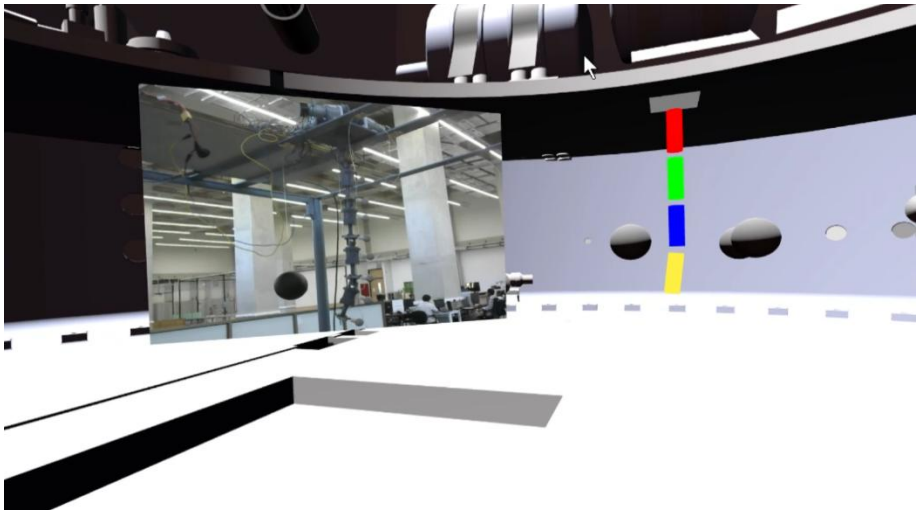
VR–Camera Hybrid Interface: The VR–camera hybrid interface presented both the virtual robot and live camera feed within the same environment. The operator was positioned 1.12 m from the URDF-based robot model at the initial position and could move within the interface during operation. The virtual camera had a field of view of 60° vertical and 84.07° horizontal. The camera feed (as described in the camera-based interface) was displayed on a Unity UI canvas positioned on the left side of the URDF-based robot model (as described in the VR-based interface), allowing simultaneous observation of both views.



a. VR Interface



b. Video Interface



c. Hybrid Interface

Figure 5. Example of Immersive Human Robot Interface

3.8. HMI Study in Microgravity

Following the literature survey and previous study undertaken at the International Space Station, we aimed to contribute to developing and evaluating graphical user interfaces for space missions. The study was reviewed by NASA IRB and determined to be Exempt under category 3(i)(B) [NASA IRB 2026]. The PI went through an online training to undertake human subject research. Informed consent was taken from all participants. The ethical declaration statement at the end of the paper furnishes further details. All methods were performed in accordance with the relevant guidelines and regulations. Figure 6 below and the supplementary material uses picture and video of astronauts available in public domain.

We reported raw data in terms of task completion times with respect to target size and distances from centre of screen that can be used to evaluate task completion times using GOMS (Goal Operator, Method, Selection) model. Three ground crews, who were test pilots and astronaut designate, and two university students also undertook the tests during the study period. We included both ground crews and students to help in setting sampling criteria during early-stage evaluation of spacecraft HMI as trained test pilots are often rare and many space programs already started training civilians as astronauts. Our study was conducted once per day for 14 days stay period at the International Space Station during June 2025 (figure 6).

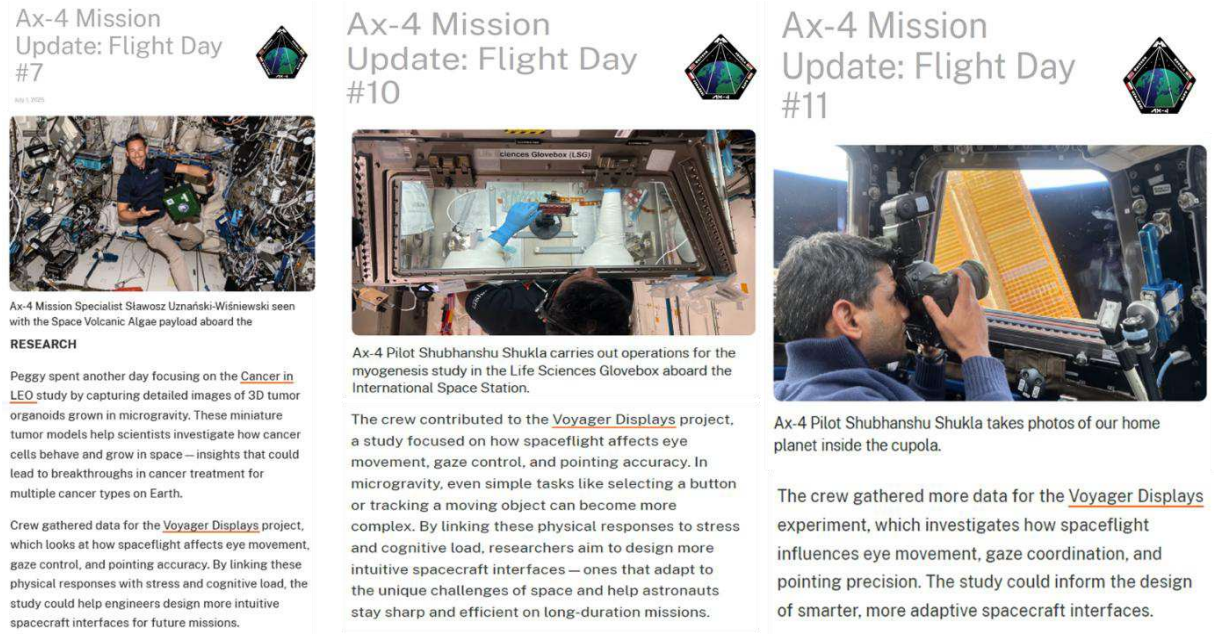


Figure 6. Screenshots from Axiom Website [https://www.axiomspace.com/missions/ax4] reporting the Voyager Display Experiment used in the Study

The tasks were designed following ISO 9241 pointing task using three different target sizes and distances

- Sizes: 20 pixels, 35 pixels and 50 pixels (5, 10, 15mm)
- Distances from centre of screen: 120 pixels, 140 pixels and 160 pixels (24, 27.5, 32mm)

The order of the pointing tasks with finger and stylus were counterbalanced in subsequent days to minimize order effect. All tasks were undertaken on an Apple iPad Pad Pro (11-inch) (3rd generation) with default screen settings in Landscape mode and finger and an Apple Pencil (version 2.0) was used for pointing. One astronaut undertook the task 11 days while a second astronaut could undertake the trial

only for two days. Table 2 below shows the number of sessions recorded from each participant. It may be noted that one session of the pointing task consisted of 60 pointing tasks. For comparing pointing times, first we calculated descriptive statistics. Figure 1 shows a boxplot of the pointing times in different conditions. Next, we removed pointing times exceeding two seconds considering those outliers. The value of two seconds was above outer fence values for all conditions. The value of 2 secs was chosen based on practical consideration of maximum duration required for completing a pointing tasks and we retained more than 99% of pointing tasks for further analysis. We averaged the pointing and selection times with respect to each combination of target size and distances as required by Fitts' Law analysis.

Table 2 Recorded session from Participants

Participants	Finger Pointing	Stylus Pointing
Astronaut 1	6	9
Astronaut 2	1	3
Ground Crew 1	8	7
Ground Crew 2	3	3
Ground Crew 3	3	3
Student 1	8	8
Student 2	7	7

The total number of pointing tasks were more than 400 for each condition. Figure 7 shows the Pointing Time vs Index of Difficulty (ID) plot. It may be noted here that the ID is calculated from the 2D screen, not the actual ID considering the distance of user from screen.

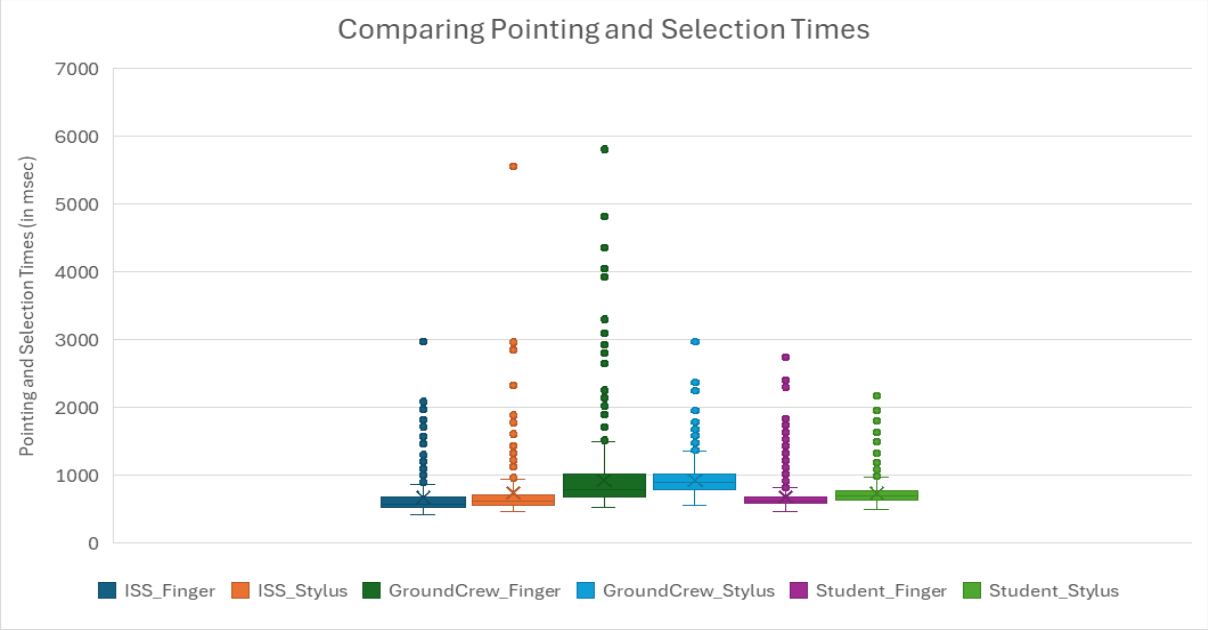


Figure 7. Box Plot of Pointing and Selection Times for different conditions

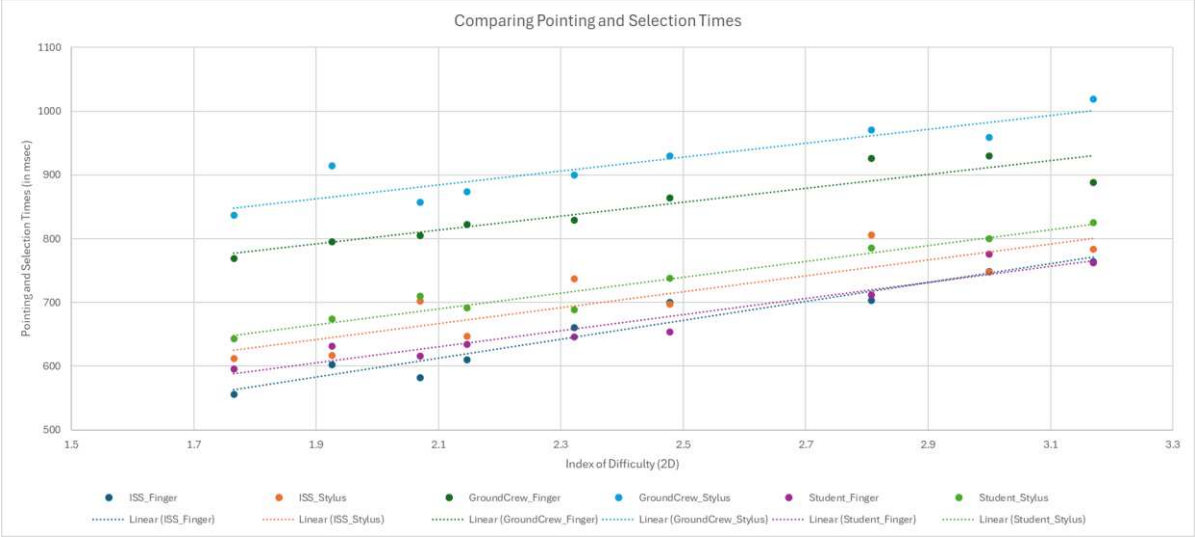


Figure 8. ID vs MT plot for different conditions

We undertook a *Participant Type(3) × Device Type (2)* ANOVA and found a statistically significant difference between pointing by finger and stylus $F(1,24)=76.32$, $p<0.001$, $\eta^2=0.76$ (figure 8). We also found statistically significant difference between ground crews and two other groups of users (ISS crews and students). Table 2 below furnishes the correlation between ID (2D) and pointing and selection times. The high value of correlation indicates that Fitts' Law holds true in microgravity and can be used to predict pointing and selection times in microgravity environment.

Table 2. Correlation between ID and Pointing and Selection Times

ISS_Finger	ISS_Stylus	GroundCrew_Finger	GroundCrew_Stylus	Student_Finger	Student_Stylus
0.97	0.88	0.93	0.92	0.96	0.98

The following equations can be used to calculate pointing and selection times for different sizes and positions of targets on a Graphical User Interface **in microgravity environment and used in the previously described VR simulator to predict task completion times of representative operations.**

Pointing time with Finger (in msec) = 148.15 $Log_2(1 + \frac{Distance\ to\ Target}{Width\ of\ Target})$ **+ 301.61 ……. Eq 1**

Pointing time with Stylus (in msec) = 124.58 $Log_2(1 + \frac{Distance\ to\ Target}{Width\ of\ Target})$ **+ 405.33 ……. Eq 2**

4. Applications

This paper proposed a Virtual Reality spacecraft simulator developed for exploring different human machine interfaces for manual operation. We investigated manual operations in past and existing spacecrafts and space stations in details. We identified several design alternatives in terms of spacecraft manoeuvring hardware, outside view orientation, human robot interfaces and so on. We implemented multiple human machine interfaces and personalization feature at the console interfaces. Earlier studies already compared different design alternatives with respect to deorbiting manoeuvre. The VR simulator is

also integrated to a physical robotic arm and real time logging software synchronized with ocular and EEG sensors for comparison of human factors in terms of task completion time and cognitive load.

4.1. Application 1 – Predicting Emergency Response Times

One uniqueness of the proposed VR simulator is it does not only allow to undertake user studies with respect to various design alternatives but also is calibrated with data collected in sustained microgravity. The NASA Virtual Reality Lab (VRL) used for astronaut extravehicular activity (spacewalk) training at the Johnson Space Centre (JSC) utilizing high fidelity six degree of freedom simulation, coupled with a set of force/moment sensors and a custom-built man-rated robot. The NASA VRL provides the response and feel of handling an object of nearly any size or mass in the zero-g environment of space. While the proposed simulator can be integrated to six DoF motion platform, but it allows to predict completion times for representative tasks in microgravity. Based on literature survey, our proposed study during the Axiom 4 mission is the first effort to calibrate Fitts' Law in sustained microgravity. The resulting equation is integrated to the VR simulator, for example table 3 below demonstrates calculation of completion time for an emergency response action using equation 1 during ascend, descent and on orbit conditions. The emergency response sequence modelled below only included pressing a set of bezel keys or touchscreen buttons in the console. Distances to target in 3D environment was accurately measured using the VR simulator before implementation of a physical mock up. A video of the sequence can be found at the supplementary video while figure 9 illustrates a representative sequence with numbered arrows below.

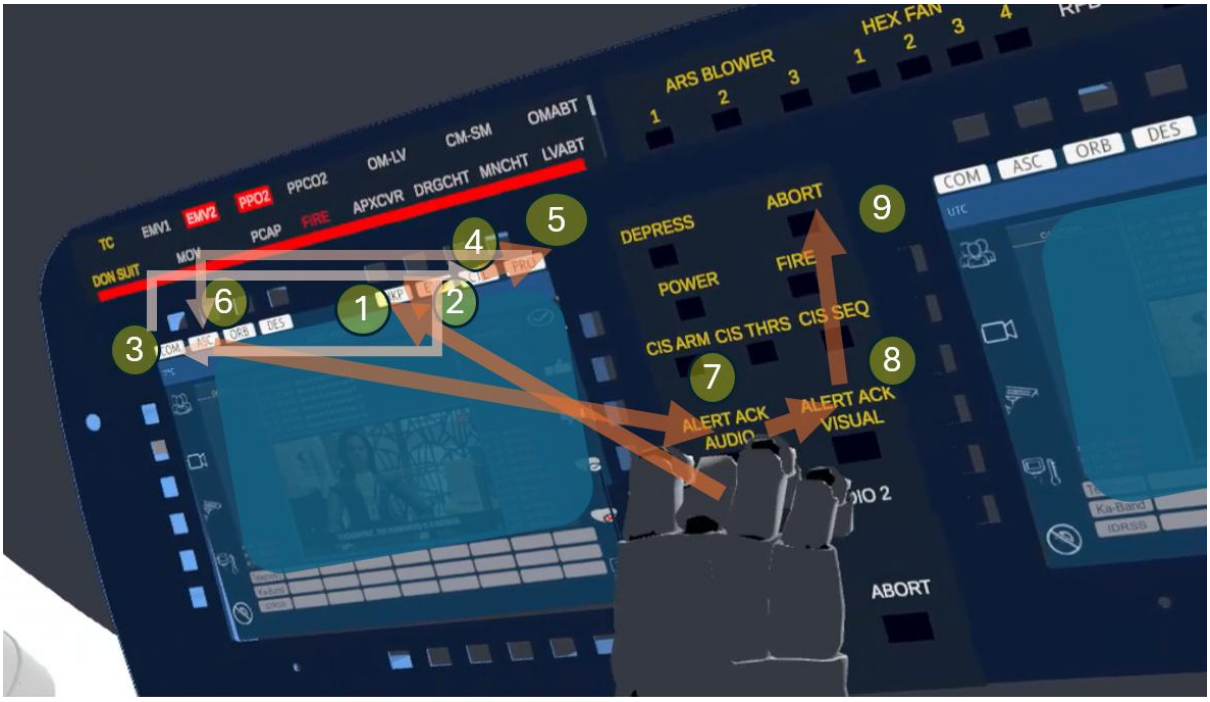


Figure 9. Action on Emergency Response during Ascent

Table 3. Calculation of Emergency Response Times during different phases

	Distance to Button (in cm)	*Width of Button (in cm)*	*Task Completion Time in Microgravity (in msec)*
During launch			
To monitor system health, press HKP (Housekeeping) button to check internal spacecraft status like temperature and voltage.	58.4	2.7	968.31
To control environmental conditions, press ENV (Environmental Control) button to manage cabin pressure and life-support systems.	3.1	2.7	465.03
To manage communication, press COM (Communications) button to control telemetry and data transmission.	21.9	2.7	773.86
To control spacecraft orientation, press CTL (Guidance, Navigation, and Control) button to manage attitude and stabilization.	25	2.7	799.22
To manage thrust systems, press PRO (Propulsion) button to control engines and fuel systems.	3.2	2.7	468.69
During launch phase, press ASC (Ascent) button to initiate or monitor upward flight operations.	25.1	2.7	799.99
On getting alert, press Audio Alert button to acknowledge audible warning signals.	37.9	1.44	1008.56
On getting alert, press Visual Alert button to acknowledge visual warning indicators	6.5	1.44	666.51
In case of emergency, press Abort button to terminate the current mission phase safely.	13.8	1.44	805.87
Total Time			**6756.05**
in orbit			
To monitor system health, press HKP (Housekeeping) button to check internal spacecraft status like temperature and voltage.	58.4	2.7	968.31

To control environmental conditions, press ENV (Environmental Control) button to manage cabin pressure and life-support systems.	3.1	2.7	465.03
To manage communication, press COM (Communications) button to control telemetry and data transmission.	21.9	2.7	773.86
To control spacecraft orientation, press CTL (Guidance, Navigation, and Control) button to manage attitude and stabilization.	25	2.7	799.22
To manage thrust systems, press PRO (Propulsion) button to control engines and fuel systems.	3.2	2.7	468.69
For orbital operations, press ORB (Orbital Operations) button to manage spacecraft activities in orbit.	22	2.7	774.72
On getting alert, press Audio Alert button to acknowledge audible warning signals.	35	1.44	992.19
On getting alert, press Visual Alert button to acknowledge visual warning indicators	6.5	1.44	666.51
In case of emergency, press Abort button to terminate the current mission phase safely.	13.8	1.44	805.87
Total Time			**6714.41**
During Landing			
To monitor system health, press HKP (Housekeeping) button to check internal spacecraft status like temperature and voltage.	58.4	2.7	968.31
To control environmental conditions, press ENV (Environmental Control) button to manage cabin pressure and life-support systems.	3.1	2.7	465.03
To manage communication, press COM (Communications) button to	21.9	2.7	773.86

control telemetry and data transmission.			
To control spacecraft orientation, press CTL (Guidance, Navigation, and Control) button to manage attitude and stabilization.	25	2.7	799.22
To manage thrust systems, press PRO (Propulsion) button to control engines and fuel systems.	3.2	2.7	468.69
During landing sequence, press DES (Descent) button to control downward trajectory and landing.	18.9	2.7	746.06
On getting alert, press Audio Alert button to acknowledge audible warning signals.	32.3	1.44	975.74
On getting alert, press Visual Alert button to acknowledge visual warning indicators	6.5	1.44	666.51
In case of emergency, press Abort button to terminate the current mission phase safely.	13.8	1.44	805.87
Total Time			**6669.29**

Application 2- User Study on Graph Monitoring Task

While the previous application highlighted the use of the VR simulator as a predictive system, the following use case highlights another application of undertaking user study to take design decision of rendering graphical elements on console. We undertook a user study investigating user preferences and cognitive load during live graph monitoring tasks in the VR simulator, addressing challenges faced by astronauts and engineers when interacting with dynamic graphical interfaces. Eight participants, divided equally between astronaut-designates and engineers, engaged in anomaly detection tasks using VR-implemented graphs with various font sizes and line widths. Cognitive load was assessed through EEG-based indices and eye-tracking metrics, alongside task accuracy. Findings indicated that interface parameters significantly impacted performance and perception; specifically, smaller fonts and thinner lines led to higher task accuracy, while larger fonts were preferred and linked to reduced cognitive load. Eye-tracking data suggested that fixation rates were influenced by line thickness and font size, revealing differing self-reported measures between participant groups. The study identified a discrepancy between user preference and actual performance, underscoring the need for adaptive, customizable interfaces and the integration of subjective and physiological evaluations in designing effective human-machine interfaces for high-stakes environments.

The task had live graphs in a virtual setting including font sizes and line widths. The graph was similar to a line graph which changes over the time, user would observe three anomalies in each graph in each console which were randomly generated. We considered three font sizes 24 (visual angle 0.89°), 36 (1.34°), and 48 (1.78°) for presenting a live value in Y-axis graph. The line width was set for the two settings 5, and 15. We

generated six conditions by selecting three font sizes and two line widths combinations and randomized order of presentations to avoid order effect. All six conditions complied to Mil 1472G standard for rendering graphical primitives.

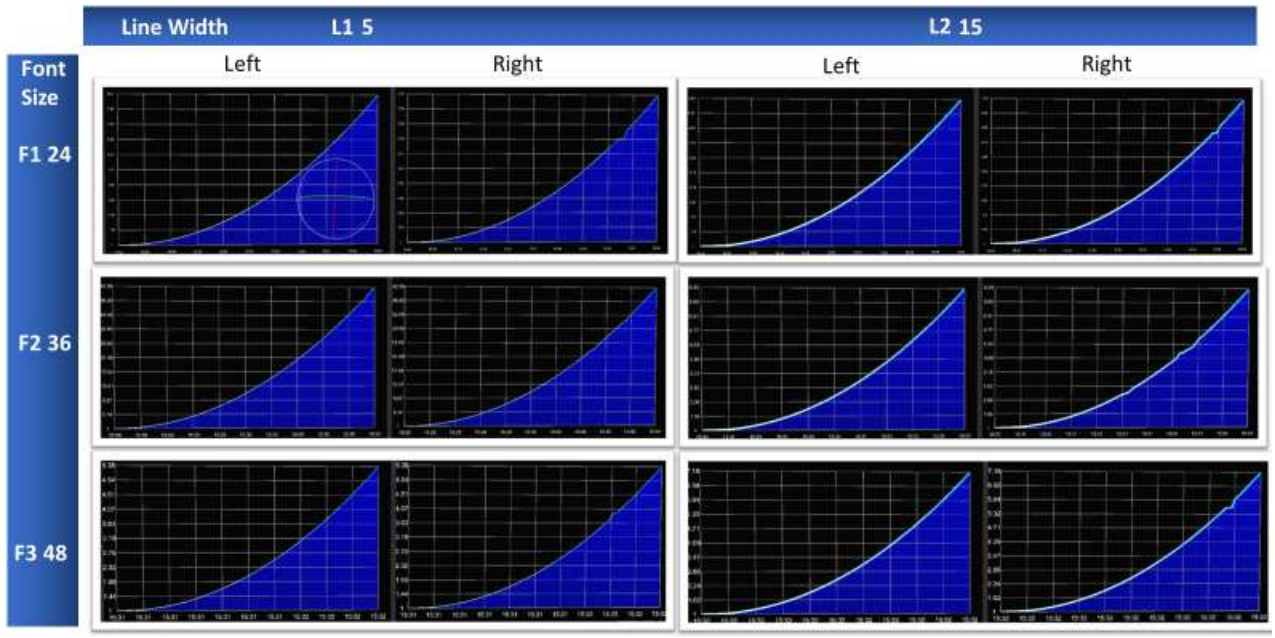


Figure 10. Graph setting in Virtual Environment

Participants underwent a preliminary test to familiarize themselves with the task, followed by calibration of the eye tracker and EEG contact quality. Each user manipulated the HTC VIVE joystick, with specific buttons designated for logging anomalies detected in visual graphs. The tasks included six randomized conditions, and participants were allowed to terminate involvement should they experience discomfort during the experiment. All participants could undertake tasks in all conditions and did not report any motion sickness or other physical problems. All participants could identify and report all anomalies. We undertook repeated measure ANOVA on all dependent variables considering participant type as a between subject factor. Mauchy's test is used to check conformity to Sphericity assumption. In the following table, we listed all significant main and interaction effects.

We found significant interaction effect of fixation rate and accuracy with respect to font size and line width of graph. While fixation rate increased with thicker line width for 24 point font size, there was opposite trend for bigger font sizes – fixation rate decreased with thicker line width. The accuracy of reporting the value of the anomaly decreased for thicker line width for font sizes 24 and 36 while it slightly increased for font size 48 and line width 15. The perceived cognitive load and usability showed similar trend with respect font size. With increase in font size the NASA Task Load Index (TLX) value decreased, and IBM System Usability Scores (SUS) values increased indicating lower perceived cognitive load and higher usability. We found significant interaction effect between participants and TLX, SUS scores. The pilots' response for different conditions did not significantly change while engineers reported lower cognitive load and higher usability for bigger font size and thicker line width.

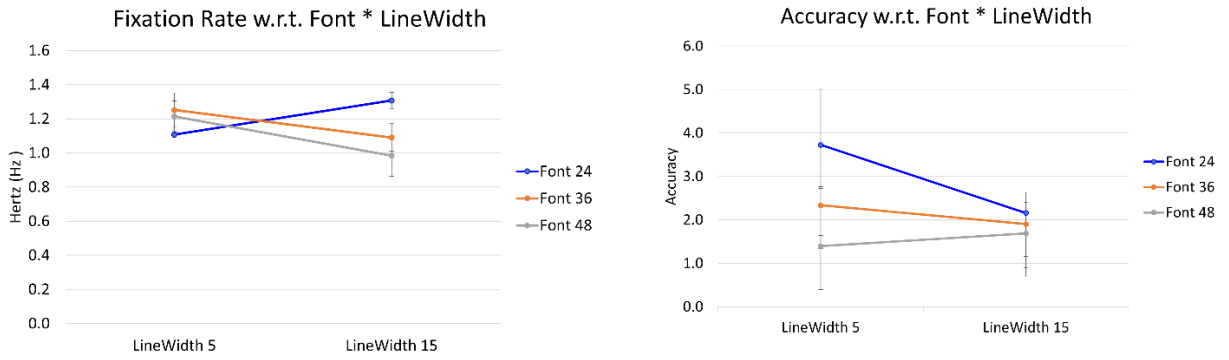


Figure 11. Comparing Fixation Rate and Anomaly Detection Accuracy w.r.t. Line Widths

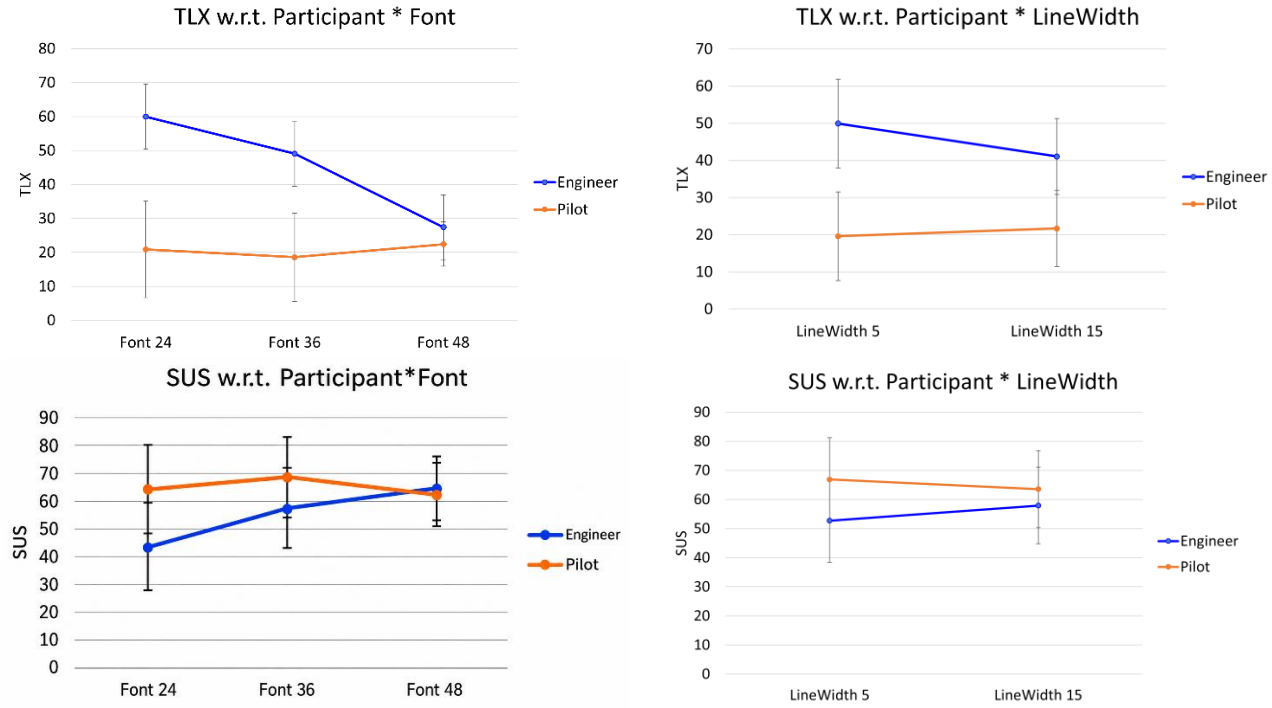


Figure 12. Comparing self-reported scores w.r.t. Font Sizes and Line Widths

The study highlighted a disparity between user preferences and performance regarding font size and line width. Users favoured larger font sizes; however, accuracy was higher with smaller sizes and widths. Notably, self-reported scales revealed significant differences between Pilots and Engineers, though physiological measures did not support these distinctions. Key lessons learned include the necessity for adjustable user interface parameters, as no single setting optimally balances preference and performance. It is essential to assess user interfaces through both self-reporting and physiological measures, given their lack of correlation. Systems evaluated solely through self-reported scales should be approached cautiously, particularly for pilots, as engineers' self-evaluations could introduce biases. The research did not identify an ideal combination of font size and line width, but it did note varied fixation rates among combinations. The findings underscore the importance of incorporating customizable settings for font size, line width, lighting, and colour to enhance readability and overall user experience.

5. Future Work

Future work is implementing docking and aerial flight of spacecraft in the VR simulator. We are also working on collecting human robot interaction data in sustained microgravity. Early missions like Gemini demonstrated purely manual rendezvous and docking using visual cues, radar-assisted targeting, and hand controllers for translation and rotation, laying the foundation for human-controlled precision operations in orbit. The Soviet Soyuz program introduced a major advancement with automated docking systems like IGLA-S, while still retaining manual override capabilities, establishing the principle of "dissimilar redundancy" that enhances safety by combining automation with human intervention. Apollo missions further refined manual docking techniques in lunar missions, while the Space Shuttle era expanded operational capability by integrating both docking and berthing, supported by camera systems, laser ranging, and the Canadarm robotic manipulator for handling payloads. With the advent of modern spacecraft such as Shenzhou, Crew Dragon, and Starliner, docking has become largely autonomous, though manual capability remains as a critical backup; notably, Crew Dragon departs from traditional joystick-based interfaces by employing touchscreen controls with augmented displays to compensate for reduced tactile feedback. In parallel, cargo resupply systems exhibit a mix of autonomous docking (e.g., Progress, ATV) and crew-assisted berthing (e.g., Cygnus, HTV), highlighting operational diversity based on mission requirements. The survey also details the evolution of robotic arms from early systems like the Shuttle Canadarm to advanced manipulators such as Canadarm2, Dextre, ERA, and Chinese station arms, which incorporate multi-modal control strategies including manual teleoperation, pre-programmed sequences, semi-autonomous execution, and ground-based control. These systems are equipped with sophisticated sensing, including cameras, force–torque sensors, and collision-avoidance algorithms, enabling precise manipulation, module relocation, and maintenance tasks while minimizing astronaut workload and extravehicular activity risks. Despite increasing automation, human-machine interfaces (HMI) remain cantered on visual feedback—either direct line-of-sight or camera-based—and dual joystick control for six-degree-of-freedom motion, with overlays providing critical spatial and kinematic information such as range, alignment, and relative velocity. Our future research will explore the shift from manual, pilot-centric operations to hybrid human-autonomy systems, where safety, precision, and efficiency are achieved through the integration of advanced automation with intuitive and reliable human control mechanisms. Representative docking and human robot interaction tasks will be implemented in the VR simulator, and comparative studies will be undertaken involving both pilots and civilians.

6. Conclusion

This paper addresses a critical gap in the aerospace industry by shifting the focus of spacecraft simulators from purely training-based models to comprehensive tools for Human-Machine Interface (HMI) design optimization. By calibrating a configurable Virtual Reality (VR) environment with actual performance data collected during the Axiom-4 mission on the International Space Station, the authors provide a unique, validated framework for predicting task completion times in sustained microgravity. The integration of multi-modal physiological sensors (EEG and eye-tracking) alongside versatile hardware controls and personalized console settings ensures that future spacecraft cockpits can be tailored to the evolving needs of both professional astronauts and the growing population of civilian space travellers.

Declarations

Financial Declaration

The study did not receive funding from any source

Human Ethics and Consent to Participate declarations

The 14 CFR 1230.104(d) refers to the section of the NASA Institutional Review Board (IRB) regulations that outlines exemptions for human subjects' research. Under 14 CFR 1230.104(d), the National Aeronautics and Space Administration (NASA) defines specific categories of human subjects research that are exempt from standard Institutional Review Board (IRB) oversight. This regulation aligns with the federal "Common Rule" implemented across multiple federal agencies to streamline low-risk research workflows. The NASA IRB office has reviewed and determined that this protocol (STUDY00000851: ANALYSING HMI IN MICROGRAVITY Initial Approval: 1/17/2025) meets the criteria for Exempt review per 14 CFR 1230.104(d). Informed Consents were obtained from all participants including astronauts, and astronaut designates through Multinational Consent Form for Spaceflight Related Participation in Human Research. All methods were performed in accordance with the relevant guidelines and regulations. Consent to publication has been received from competent authorities of ISRO.

Competing Interest

Authors do not declare any competing interest.

Author Contribution

- AK implemented majority of the simulator and designed user studies.
- ST, SS, HV, MK helped in implementing tasks the VR Simulator.
- MM and KPS implemented the web-based application for data collection in Microgravity.
- PB supervised the study and analysed results.

Acknowledgement

This study was conducted as part of the experiment titled 'Analysing Human Interaction with Electronic Displays in Microgravity' selected by ISRO's Human Space Flight Center (HSFC) for ISRO-NASA joint mission to the ISS (Axiom-4 mission). Authors are grateful to HSFC/ISRO for enabling this study during the Axiom-4 mission.

References

[1] Bieg, T., Reisinger, M., Fröhlich, P. (2024) Task performance with touchscreen interfaces under conditions of head-down tilt bed rest. CEAS Space J 16, 333–349

[2] Ciofani G., Lombardo V., Mazzei D., Migliore A., Carrozza M.C., Dario P. and Micera S. (2012), Verification of Fitts' Law in Different Gravitational Environments, Proceedings of the 57th International Astronautical Congress

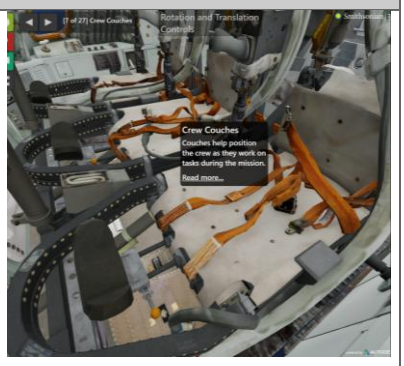
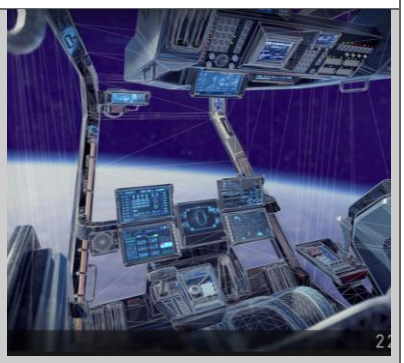
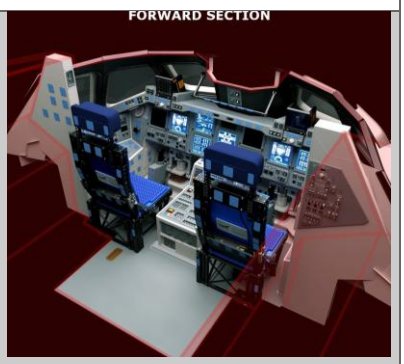
[3] Cross JI, Ryley T. (2025), Assessing evidence-based training in a collaborative virtual reality flight simulator. The Aeronautical Journal. 2025;129(1332):261-281. doi:10.1017/aer.2024.113

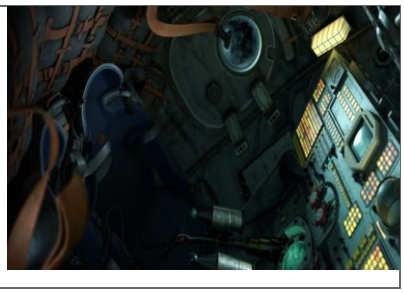
[4] Eliott D, Helsen WF, and Chua R (2001). A century later: Woodworth's (1899) two-component model of goal-directed aiming. Psychological bulletin, 127(3):342, 2001

[5] Fitts P. M. (1954). The information capacity of the human motor system in controlling the amplitude of movement. Journal of Experimental Psychology, 47, 381–391

[6] Granados-Cruz LG, Chávez-Moreno RG, Ferrer-Perez JA, Romo-Fuentes C, Ramírez-Aguilar JA (2023), Historical review of simulators for satellite position and orientation control, International Conference on AeroSpace Science and Technology, IOP Publishing
[7] Hockey, G. R. J. (1997). Compensatory control in the regulation of human performance under stress and high workload: A cognitive–energetical framework. *Biological Psychology*, 45(1–3), 73–93. https://doi.org/10.1016/S0301-0511(96)05223-4
[8] Holden K, Greene M, Cross V, Sandor A, Thompson S, Feiveson A, Munson B (2023), Effects of Long-duration Microgravity and Gravitational Transition on Fine Motor Skills, Human Factors 65 (6), pp 1046-1058
[9] India will have its own Space Station by 2035, which will be known as "Bharatiya Antriksh Station, Available at: https://www.pib.gov.in/PressReleaseIframePage.aspx?PRID=2068495&reg=3&lang=2, Accesses on 30th April 2026
[10] ISO 9241-303:2011, Ergonomics of human-system interaction – Part 303: Requirements for electronic visual displays
[11] Krishnan A, Vishwakarma H, Chutani D, Atulkar AA, Bhatad D, Kharsade M and Biswas P (2025), Human-in-the-Loop Spacecraft Maneuvers: Investigating Human Factors Through VR and Machine Learning, IEEE Space, Aerospace and Defence Conference (SPACE)
[12] Krishnan A, Vishwakarma H, Kharsade M and Biswas P (2024), Comparison of View Orientation in Manned Spacecraft Through Virtual Reality Simulation, IEEE Space, Aerospace and Defence Conference (SPACE)
[13] MacKenzie IS (2018), Fitts' Law, The Wiley Handbook of Human Computer Interaction, Volume 1, First Edition. Edited by Kent L. Norman and Jurek Kirakowski, John Wiley & Sons Ltd.
[14] MacKenzie, I. S., Kauppinen, T., & Silfverberg, M. (2001, March). Accuracy measures for evaluating computer pointing devices. *In Proceedings of the SIGCHI conference on Human factors in computing systems (pp. 9-16).*
[15] Metodi TS(2010), Space Vehicle Testbeds and Simulators Taxonomy and Development Guide, Aerospace Report No. TOR-2010(8591)-16. Prepared for USA Space and Missile Systems Center, Air Force Space Command
[16] MIL-STD-1472G (2012), US Department Of Defense, Design Criteria Standard, Human Engineering
[17] NASA Simulations Improve Artemis II Launch Environment, Available at: https://www.nasa.gov/aeronautics/artemis-sls-launch-sim/, Accesses on 30th April 2026
[18] NASA Space Flight Human-system Standard, Volume 2, rev A (2025): Human Factors, Habitability, And Environmental Health
[19] NASA Virtual Reality Lab, Available at https://www.nasa.gov/virtual-reality-lab-doug/, Accessed on 27th April 2026
[20] NASA. (2017). NPR 8705.2C Human Rating Requirements for Space Systems
[21] NASA IRB Submission Guidance (2026), Available at https://www.nasa.gov/irb-submission-guidance/, Accessed on 16th May 2026
[22] SPHERES International Space Station National Laboratory Facility, Available at https://www.nasa.gov/wp-content/uploads/2017/12/spheres_fact_sheet-508-7may2015.pdf, Accessed on 27th April 2026
[23] Wilde M, Clark C, Romano M (2019), Historical survey of kinematic and dynamic spacecraft simulators for laboratory experimentation of on-orbit proximity maneuvers, Progress in Aerospace Sciences, Volume 110

Appendix 1 – Existing VR Models for Spacecraft Cockpit

Name	Format	Obtained From	Picture
Apollo 11	.blend, .fbx	Smithsonian 3D (https://3d.si.edu/object/3d/command-module-apollo-11:d8c63e8a-4ebc-11ea-b77f-2e728ce88125)	
Sci Fi Spaceship Cockpit 4 Low-poly 3D model	.max, .fbx, .obj, .3ds	Vattalus Assets (https://www.artstation.com/vattalusassets/store/Nr22/sci-fi-spaceship-cockpit-4-low-poly-3d-model)	
Sci Fi Cockpit Heavy Fighter	.fbx, .psd	Vattalus Assets (https://www.artstation.com/vattalusassets/store/WrMJ/sci-fi-cockpit-heavy-fighter-low-poly-3d-model)	
SPACE SHUTTLE COCKPIT (HIGH POLY)	.blend	TurboSQUID (https://www.turbosquid.com/3d-models/space-shuttle-cockpit-3d-obj/833432)	

Soyuz MS-01 Interior Model	.fbx, .obj	ArtStation - Nico Kleinert (https://www.artstation.com/marketplace/p/8kVe/soyuz-ms-01-interior-model)	

Appendix 2- Usability Evaluation Methods

This appendix explains a set of parameters and algorithms to measure human factors for interactive tasks. We aimed to create one common platform to evaluate the usability of new technologies / devices for humans which will give a better index of usability.

List of Equipment

1. Emotiv EPOC FLEX 32 Channel EEG Tracker
2. HTC Vive Eye Pro Virtual Reality System with integrated eye gaze tracker
3. Eye Gaze Trackers (Tobii Pro Glasses, Pro X3, Eye5, 4C and EyeX) with analysis software

Physiological Parameters

A comprehensive set of dependent parameters consisting of quantitative, qualitative, and physiological variables can be measured to evaluate usability. These parameters and the related analysis methods have been described in detail in the subsequent paragraphs. Table A1 indicates the category and indication of the dependent parameters. These tools should be used along with standard self-reporting tools like NASA TLX, IBM SUS, BWS and Cooper Harper Rating.

Table A1 Summary of dependent parameters

Parameter Name	Indication
Task Completion Time	User performance
Task Specific Parameters/Accuracy measures	
NASA TLX score	Subjective indicator of cognitive workload
EEG based Task Load Index	Relative indicators of cognitive workload
Ocular parameters: **Fixation rate** **Average fixation duration** **Average saccade velocity**	
EEG based Task Engagement Index	Relative indicator of sensory processing and attention resources

Task Completion Time: The time required to complete the given task.

Task Specific Parameters: These are specific to the task such as accuracy measures, error count, etc.

EEG Processing

Electroencephalography (EEG) utilizes electrodes on the scalp to assess brain activity and cognitive workload, as evidenced by various studies. In our user research, the Emotive EPOC Flex system was

employed, with electrodes prepared in saline solution and arranged according to the standard 10-20 configuration for optimal measurement quality. Data collection yielded raw EEG values and average band power for each of five frequency bands: theta, alpha, beta-low, beta-high, and gamma. The median power for each band was calculated and visualized using topology maps in MATLAB. The ratio of the mean frontal midline theta energy to the mean parietal alpha energy is defined as the Task Load Index (TLI). It has been shown to increase overtime during different cognitive tasks. The Task engagement index (TEI) is defined as the ratio of beta band power to sum of theta and alpha band power. Average beta, alpha and theta bands of F4, F3, F7 and F8 electrodes were considered to compute TEI. TEI reflects information gathering, visual processing, and allocation of attention as it tracks the demand for sensory processing and attentional resources. Figure A1 shows the electrodes considered for TLI and TEI respectively in a topological map. For TLI, the frontal theta electrodes are highlighted in red color while the parietal alpha electrodes are highlighted in blue color. For EI, the frontal electrodes considered are highlighted in black color. The pseudo code of the TLI and TEI analysis algorithm [Krishnan 2024] is shown in Algorithm 1. The TLI and TEI values were calculated for every mode based on the EEG data of every participant.

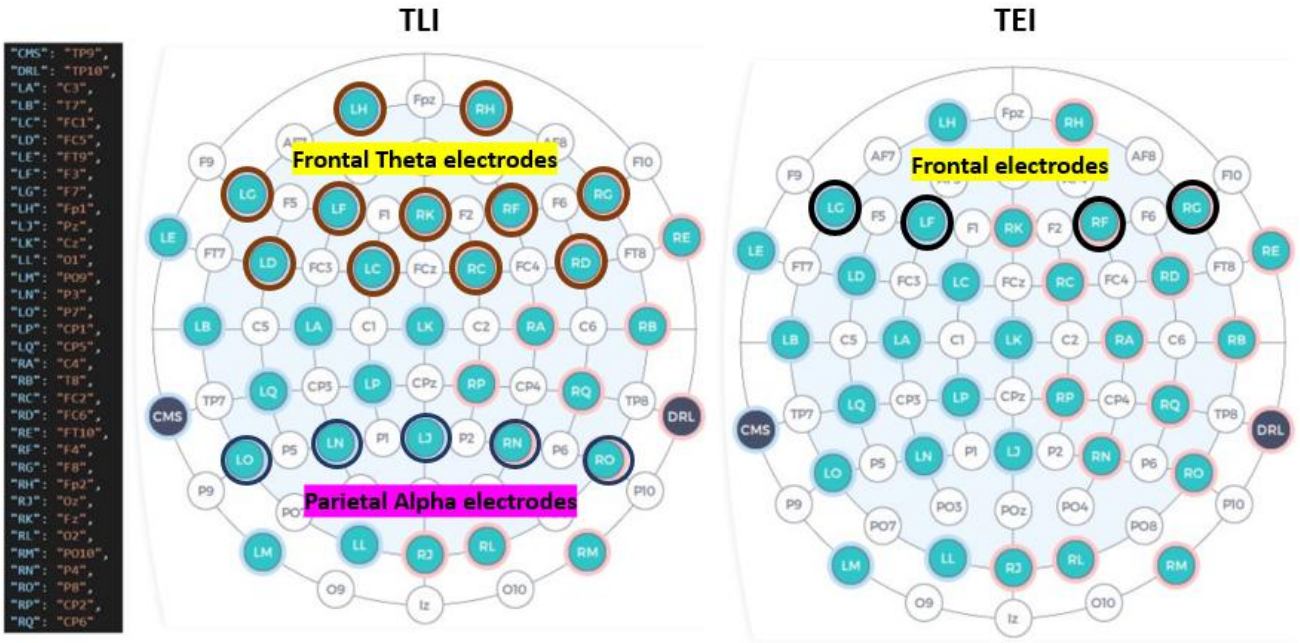


Fig. A1 EEG electrodes considered for TLI and TEI calculation

ALGORITHM 1: Algorithm for Calculating TLI and TEI from EEG Data

Input: Raw EEG values for 32 channels

Output: TLI

For each electrode

Sample raw EEG values through Hanning Window and Fast Fourier Transform

Band power averaged over 16 samples

For each sample of band power

Calculate intermediate TLI as mean (theta - Fz, Fp1, Fp2, F3, F4, F7, F8, FC1, FC2, FC5, FC6) / mean (alpha - Pz, P3, P4, P7, P8)

Calculate intermediate TEI as mean (beta - F3, F4, F7, F8) / {mean (alpha - F3, F4, F7, F8) + mean (theta – F3, F4, F7, F8)}

Compute median of set of intermediate TLI and TEI

Return TLI and TEI corresponding to respective participant and experiment mode

End

Ocular Parameters Processing

Saccadic eye gaze movement is characterized by two key types of eye movement: saccades, which quickly reposition the fovea between points of interest, and fixations, where the eye remains aligned with a target to allow processing of image details. Human perception is largely influenced by the interplay of these movements, as information is primarily gathered during fixations due to the poor image quality during saccades. The identification of fixations and saccades relies on the velocity threshold fixation identification method (I-VT), which classifies gaze points based on their velocities in degrees per second. A point is classified as a fixation if its velocity is below a set threshold of 30º/sec; otherwise, it is marked as a saccade. After classification, a clustering algorithm consolidates successive fixations and saccades, enabling an assessment of total durations, fixation rates, average fixation durations, and average saccade velocities. These metrics provide a comprehensive understanding of gaze dynamics during visual tasks. The pseudo code of the I-VT algorithm is shown in Algorithm 2. These parameters were calculated for every mode based on the eye gaze data of every participant.

ALGORITHM 2: Algorithm for Calculating Ocular Parameters from Eye Gaze Data

Input: Normalized gaze vectors (X, Y, Z) and corresponding timestamps

Output: Fixation rate, average fixation duration, average saccade velocity

For each timestamp

Calculate angle between current and immediately preceding gaze vectors (0 for first timestamp)

Calculate angular velocity as angle / time difference between the respective sample points

Label each point below velocity threshold as a fixation, otherwise as a saccade

Group successive fixations into one fixation and successive saccades into one saccade

Count total number of such fixations and saccades

Calculate total duration associated with every such fixation and saccade

Calculate task duration as sum (individual duration of each fixation and saccade)

Calculate fixation rate as total number of fixations / task duration

Calculate average fixation duration as sum (individual fixation durations) / total number of fixations

For each saccade

Calculate angle between current and immediately preceding gaze vectors (0 for first timestamp)

Calculate angular velocity as angle / time difference between the respective sample points

Calculate average saccade velocity as sum (individual saccade velocities) / total number of saccades

Return fixation rate, average fixation duration and average saccade velocity

End

Gaze distribution analysis

Spatial gaze distribution patterns are sensitive to variations in cognitive load. In general, low workload is associated with more deterministic and repetitive visual scanning patterns. Nearest neighborhood index (NNI) is an indirect cognitive workload estimator to analyze distribution of gaze position. Nearest neighbor

distance computed as the distance between each gaze point to the next gaze point near it. A higher value of NNI denotes that visual scanning is more randomly distributed in space.

NNI is the computed as the ratio of mean of nearest neighbor distance (dNN) to mean random distance (dMRD).

$$NNI = \frac{d_{NN}}{d_{MRD}}$$

Where $d_{NN} = \sum_{i=1}^{N} min[\frac{\sqrt{(fx_i - fx_j)^2 - (fy_i - fy_j)^2)}}{N}]$ and $d_{MRD} = 0.5\sqrt{Area\ of\ interest/N}$

Area of interest is computed as the rectangular area that the x and y gaze coordinates cover. fx and fy are the x and y eye coordinates respectively; and i and j are the successive time instances in x and y. N is the total number of data points.

Analysis of Results

The normality of the paired differences for each dependent parameter was checked and verified using the Shapiro-Wilk test for normality. Pairwise two tailed t-tests were then performed between the datasets for each of the dependent parameters. The statistical significance level was set at 5% (α=0.05). Cohen's d was calculated as a measure of effect size. Descriptive statistics such mean and standard deviation were calculated and visualized for each dataset. The analyses were performed using the Data Analysis Toolpak in MS-Excel and IBM SPSS software (Version 24). In our study, we generated one datapoint per user per condition where each row of physiological parameter came from one participant. Considering that each participant is a highly trained test pilot, sequence of task conditions was regularly interchanged to avoid order effect and brief relaxation period was allowed between consecutive simulations; we assumed independent observation across data points for the analysis.

Supplementary Files

This is a list of supplementary files associated with this preprint. Click to download.

- I3DSpace.mp4